KSCE Journal of Civil Engineering (2023) 27(11):4787-4797
DOI 10.1007/s12205-023-1732-2

pISSN 1226-7988, eISSN 1976-3808
www.springer.com/12205

Structural Engineering

Study on the Safety of Tunnel Structure Vibration in Dry Ice Powder Thermal Shock Rock Breaking

Xiaofei Wang[a], **Shaobin Hu**[b], **and Enyuan Wang**[a]

[a]*School of Safety Engineering, China University of Mining and Technology, Xuzhou 221116, Jiangsu, China*
[b]*College of Civil and Transportation Engineering, HoHai University, Nanjing 210098, Jiangsu, China*

ARTICLE HISTORY

Received 22 September 2022
Accepted 13 July 2023
Published Online 8 September 2023

KEYWORDS

Dry ice powder thermal shock rock breaking
Vibration measurement
Hilbert huang transform
Tunnel excavation

ABSTRACT

The application of explosive blasting for rock breaking works was not possible in densely populated areas, which caused problems in urban tunnel construction. In the application of dry ice powder thermal shock breaking in tunnel excavation, a vibration monitoring system was employed to monitor the vibration response of the tunnel structure during the breaking process, and it was used to extract the signal characteristics by Hilbert-Huang transformation. Experimental results are as follows: 1) The peak vibration speed was below 50 mm/s for concrete structures safe as long as it was farther than 10 m from the burst hole in the support concrete. 2) Aggregate decay of vibration velocities caused by thermal shock breaking of rock with dry ice powder corresponded to the decay law of the power function. The range of influence of the vibration was considerably smaller compared to that of drilling and blasting the rock; 3) The new rock-breaking technology induced damage can be divided into three regions, with radial fractures generated by high-energy fluids dominating. 4) Hilbert Huang transform extracted signal features more objectively and accurately, with excellent reference for the safety monitoring of tunnel structures.

1. Introduction

With the development of the economy, an increasing number of tunnel projects require construction, and a large amount of rock breaking work needs to be carried out (Wu et al., 2021). The drilling and blasting method can be used for large-scale, high-efficiency rock breaking, but its application in tunnel construction was increasingly restricted due to the shortcomings of strong vibration, excessive noise and dust (Xia et al., 2018). In sensitive areas where public transport and people were densely packed, the drilling and blasting method was not available, while the mechanical rock-breaking method could not resolve the construction problems of safe and effective tunnelling due to its loud noise and low efficiency (Li, 2021). It was therefore urgent to find a new rock-breaking technique to replace the drill and blast method. Presently Carbon dioxide phase change fracturing was considered to be a promising new excavation technique with many advantages over drilling and blasting (Chen et al., 2017; Yang et al., 2020). Exploitation of gas phase changes to fracture rock emerged in the 1850s and was first tested in the field by British engineers (Wang and Konietzky, 2009). The primary process was to fracture rock by heating liquid carbon dioxide by a heater, causing it to warm up and expand, and releasing a supercritical state of high-energy carbon dioxide fluid by rupture of the carbon dioxide fracturing tube. A number of scholars studied this technique extensively as it is currently used to fracture and increase the permeability of coal in order to improve the efficiency of coal seam methane extraction (Goodarzi et al., 2015; Wen et al., 2019; Chen et al., 2020; Li, 2020a; Li et al., 2020b; Chang et al., 2023). Conventional CO_2 phase change cracking tubes were prohibited due to splash and burst accidents, and high-pressure vessels were not allowed access to construction sites (Wang et al., 2023). Hu et al. (2019) designed a new dry ice powder pneumatic fracturing rock breaking process by inventing a CO_2 energizer with independent intellectual property rights.With a large amount of heat supplied, dry ice powder phase change fractured rock was intrinsically safe.

Destruction of rock in drilling and blasting, mechanical rock breaking and dry ice thermal shock breaking unavoidably caused vibrations on the opposite side of the rock, and surrounding

CORRESPONDENCE Shaobin Hu hsbhhu@126.com College of Civil and Transportation Engineering, HoHai University, Nanjing 210098, Jiangsu, China

residences and infrastructure were damaged by the vibration disturbance (Xia et al., 2018; Huang et al., 2019; Kumar and Mishra, 2020). A number of scholars investigated the effects of blasting vibration in tanks on tunnel structures. Research indicated that maximum vibration was an important parameter for measuring vibration damage, but considering only the maximum vibration velocity was one-sided (Lee et al., 2016; Wang et al., 2022a). The further analysis of vibration data allowed for a more comprehensive analysis of the damage caused by vibration (Umit, 2008; Huang et al., 2019; Xia and Jiang, 2019). The Fourier transform required the signal to be periodic and stable. The vibration signal was dynamic, and the Fast Fourier Transform could not achieve the desired result (Tao et al., 2008). Wavelet transform was limited by Heisenberg's inaccuracy principle and the signal features could not be extracted objectively (Babu, 2008). Hilbert Huang transform composed mainly of a pre-decomposition and a post-transformation, which allows a more objective and accurate analysis of the signal as no artificial choice of window function was required (Wu and Huang, 2004). The HHT signal analysis technique was highly valuable for non-linear signals and can further improve the accuracy of the application. Applications of HHT were already reported by scholars in medicine, finance and geology (Skeberis et al., 2015; Wang et al., 2022b).

There were more studies on the vibration safety analysis of tunnel excavation drilling and blasting method, but the literature examining the structural safety of the new technology was rarely reported. The new dry ice powder thermal shock rock breaking had a good prospect of application in tunnel construction. It was urgent to study the damage of vibration on tunnel structure. For tunneling in the densely populated areas of the Nanjing Jiangbei New District, dry ice powder was used to break the rock. Vibration and noise on the support ridges were monitored. The safety of the tunnel structure was assessed by HHT analysis of the vibration model characteristics.

2. Experiment

2.1 Field Trials

As illustrated in Fig. 1, the test site is Yanshan Avenue tunnel in Pukou District, Nanjing City, Jiangsu Province. The main lithology of the rocks in the vicinity of the tunnel is sandy mudstone and the main mechanical parameters are shown in Table 1. The tunnel construction area was adjacent to the village of Puchang and was densely populated. The nearest residential houses were only 30 meters away from the tunnel construction section. As a result, the tunnel construction team mainly relied on pickaxes to break the rock, causing serious noise pollution. Complaints had been received from the neighboring residents and hotels and the construction progress was slow.

Fig. 1. Test Site

Table 1. Physical and Mechanical Properties of the Specimens

Density (g/cm^3)	Uniaxial compressive strength (MPa)	Mean shear wave velocity (m/s)	Shear strength (MPa)
2.56	22.81	21.55	2.90

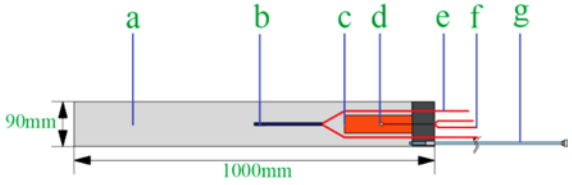

Fig. 2. Structure Diagram of L-1000 Dry Ice Powder Cracker (a: dry ice powder cabin b: heating rod c: CO2-EA d: detonator e: heating wire f: detonating wire g: safety conduit)

2.2 Stone Crushing Equipment and Technology

Figure 2 showed the internal structure of the dry ice fracturing cylinder. The dry ice cracking cylinder has a diameter of 90 mm and a length of 1,000 mm. The main structure includes a dry ice powder compartment, heating rod, CO_2 energiser, detonating agent, heating rod, wires and safety flaps. Excitation of the agent exotherm caused by the use of an initiator to cause a phase change in the dry ice powder to occur.The safety conduit can be connected to an external sensor to monitor internal pressure and can be deflated in the event of unsuccessful excitation.The CO_2 energizer used is the core technology and has completely independent intellectual property rights. Different from the traditional CO_2 phase change cracking technology, it is completely non-explosive and the reaction generates a high temperature of over 3,000°C. The specific physical and chemical parameters are shown in Table 2.

Table 2. Basic Physical and Chemical Parameters of the CO_2-EA (Hu et al., 2019)

Material	Apparent density (g/mL)	Porosity	Specific surface area (m^2/g)	Heat of combustion (kJ/g)	Thermal conductivity (W/m k)
CO_2-EA	0.12	0.92	240	21.33	0.016

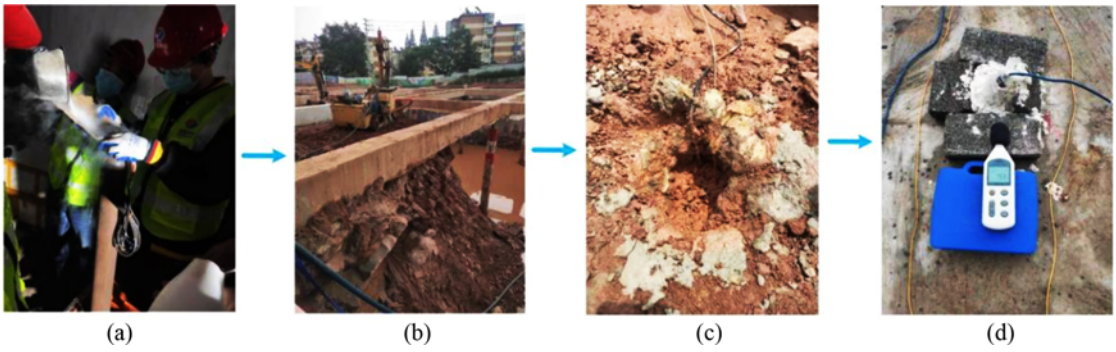

Fig. 3. Experimental Steps Diagram: (a) Assemble the Fracturing Tube, (b) Drilling, (c) Seal the Hole, (d) Arrange the Sensors

When the rock braking pressure was reached, a large amount of high energy gas was released to impact and compress the surrounding rock, creating an impact. The damage created an initial fracture and then the high energy gas expands the fracture and breaks the rock. The experimental process is shown in Fig. 3, including four steps of dry ice cracking cylinder assembly, drilling, sealing and sensor arrangement.

2.3 Inspection Network Layout

2.3.1 Instrument Description

The vibration monitoring equipment used in the test was the KJ521 vibration monitoring system manufactured by Foan Technology Ltd. It's hardware consisted of a data acquisition instrument, signal amplifier, junction box, piezoelectric vibration sensor and computer. The system could collect 16 measurement points at the same time with a sampling frequency of 1,000 Hz and an AD conversion of 24 bits. The system software comprised a vibration signal acquisition system, a vibration data processing system and a vibration data analysis system, which are responsible for acquiring, processing and analyzing vibration data respectively, and can automatically pick up vibration trigger time and end time, vibration source location and energy calculation. The AR-824 noise meter was used to collect the noise and the MAX mode can be set to obtain the peak noise level during rock breaking.

2.3.2 Location of Measurement Points

Details on the layout of the sensors as illustrated in Fig. 4,with a total of 8 sensors and 1 noise meter. V2-V8 were placed on the support ridge and V1 was placed on the concrete path. V2, V3 and V4 were placed on the support ridge close to boreholes H1 and H2. V4 was only 2.5 m from borehole H1 at its closest point. V5-V8 were placed on the second support ridge to the left of the borehole in that order. V8 was placed directly above the steel support ridge, which

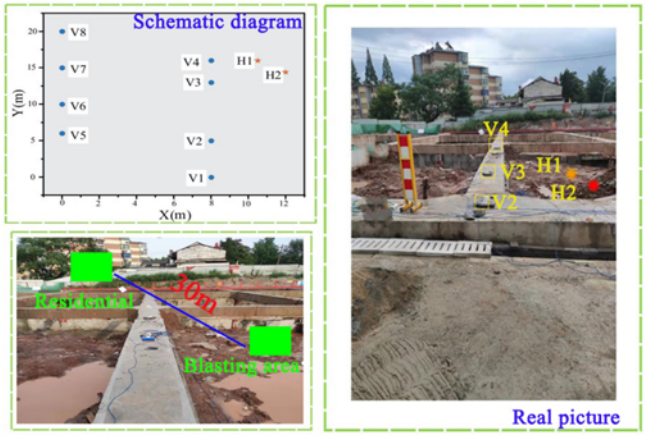

Fig. 4. Schematic Diagram of Sensor and Dry Ice Fracturing Tube Layout

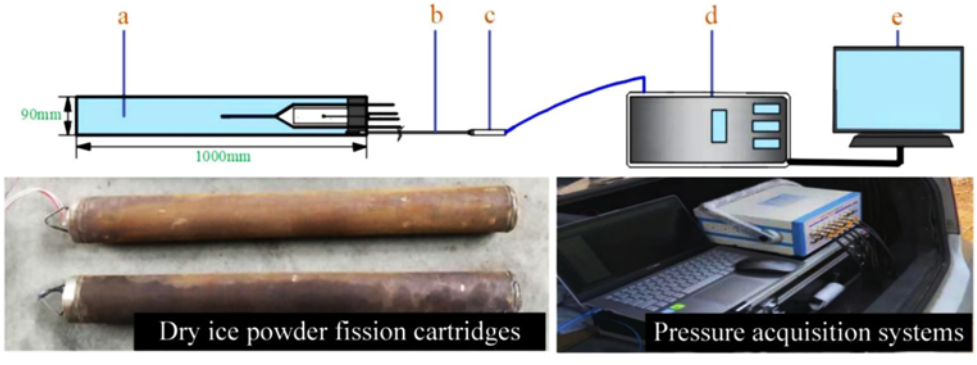

Fig. 5. Pressure Test Test System (a: dry ice powder fracturing tube; b: safety valve; c: pressure transducer; d: data acquisition instrument; e: computer)

was just above the junction of the beam and vertical beam. The noise meter was placed together with the V3 sensor, 8.38 m from H1 and 7.55 m from H2. Plaster was used as a coupling agent to fully couple the transducer to the support and the noise meter used a sponge head to filter other sound sources.

2.4 Pressure Test Experiments

Experimentally obtained peak gas pressures for dry ice thermal shock were obtained by pressure measurement. The pressure measurement experimental system was illustrated in Fig. 5. We used a special connector to connect the pressure sensor to the dry ice powder fracturing tube safety valve and a data acquisition instrument to collect and record the pressure. The pressure monitoring system consists of a pressure transducer, an 8-channel transient pressure collector and a computer to monitor the pressure inside the dry ice fracturing tube during the test. 8-channel transient pressure collector model sqcp-USB-8, with a sampling frequency of 0.25 MHz to 2.0 MHz, was selected for the 0.25 MHz mode. The pressure transducer is a cyg140f (0 – 60) with a range of 0 – 60 MPa and a response frequency of 20 kHz. the pressure collector is connected to the computer via a USB connector. the high frequency pressure transducer signal is susceptible to external signal interference and unnecessary electrical equipment is avoided during the experiments. A 6 mm conduit was used to ensure a smooth air path and to prevent any local loss of fluid to the test. A total of three experiments were carried out and test curves were obtained.

3. Test Results

3.1 Shock Beam and Sound Level from Crushed Stone

Figure 6 is the vibration waveform diagram of the first burst pipe rock breaking. With increasing distance, the fluctuation duration of the vibration waveform gradually decreased to about 0.5 s. With increasing focal length, the peak time of the vibration waveform was gradually delayed as the vibration propagated from near too far. At the same support ridge, the peak value of the vibration waveform gradually reduced with increasing distance from the source. However, V8 showed a higher peak value of vibration than V4 which was closer to the source. The reason for this was that V8 was at the intersection of the supports and there was a steel frame directly below the ground, which would have accelerated the transmission of vibration. The second path on the left was not connected to the ground, resulting in less vibration attenuation. The maximum noise values for the two dry ice cracking cylinders breaking rock were 79.3 dB and 82.5 dB as a result.

3.2 Fast Fourier Transform Spectrum Analysis

As shown in Fig. 7, the Fourier transform was applied to the V4, V8, V3 and V2 sensor waveforms from the first rock-breaking vibration. The Fast Fourier Transform process converted the value of the signal energy manifested in time to a value at a different frequency. It was evident from the results that the signal in each frequency band disappears partially as one gets further away from the point where the vibration occurs, with the higher frequency portion of the signal disappearing more quickly.

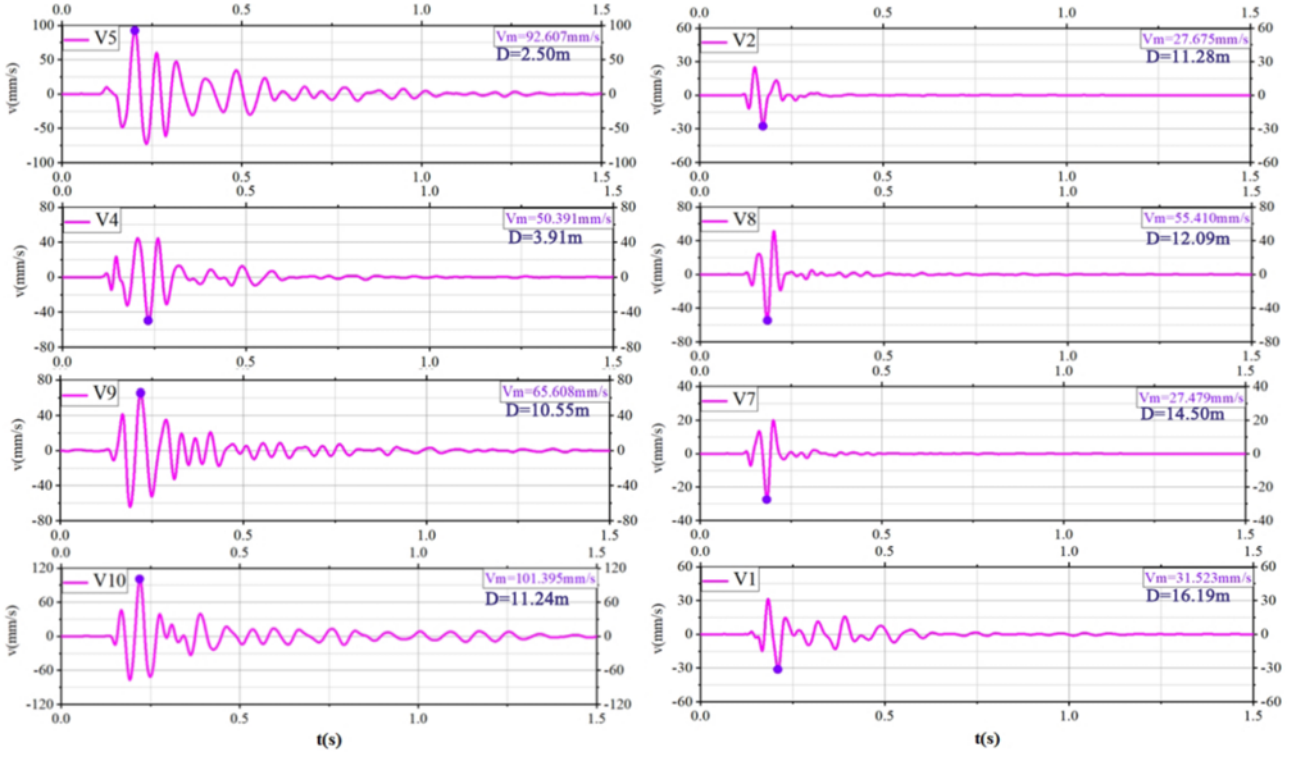

Fig. 6. Vibration Measurement Waveform of First Shot

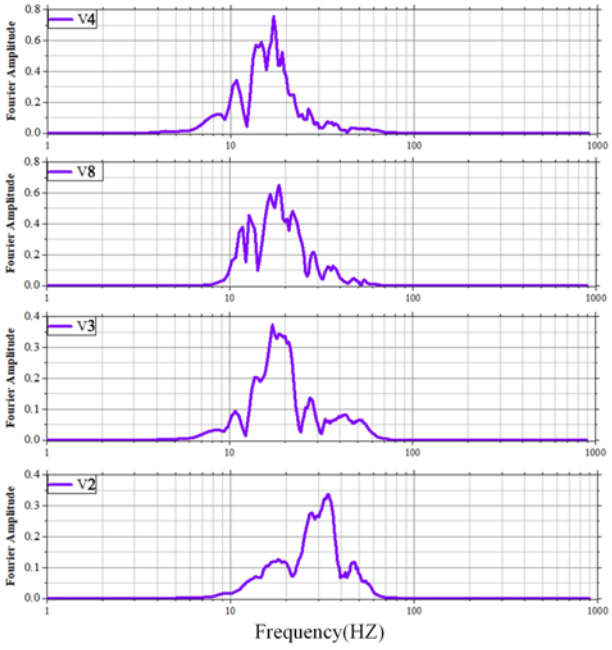

Fig. 7. Fourier Spectrum Diagram of First Shot

Numerous frequencies of vibration with the same frequency of self-oscillation of the rock mass were reduced by resonance.

3.3 Results of Hilbert-Huang Transformation of Signals

The Hilbert Huang transform spectral analysis method was proposed by Norden E. Huang et al. It consists of two main steps, decomposition and analysis. Signal decomposition refers to empirical mode decomposition, which does not require a priori functions and is more objective than wavelet analysis. Hilbert spectral analysis first transforms the signal components into a spectrum and finally merges them to obtain a spectrogram of the original signal.

3.3.1 Analysis of the EMD Decomposition of the IMF Component

As shown in Fig. 8, the vibration waveforms of the V4, V3 and V2 sensors were decomposed by EMD into IMF components, each with similar characteristics to the original signal. Initial decomposition was achieved with the highest component energy and at a high frequency, indicating that the decomposition was

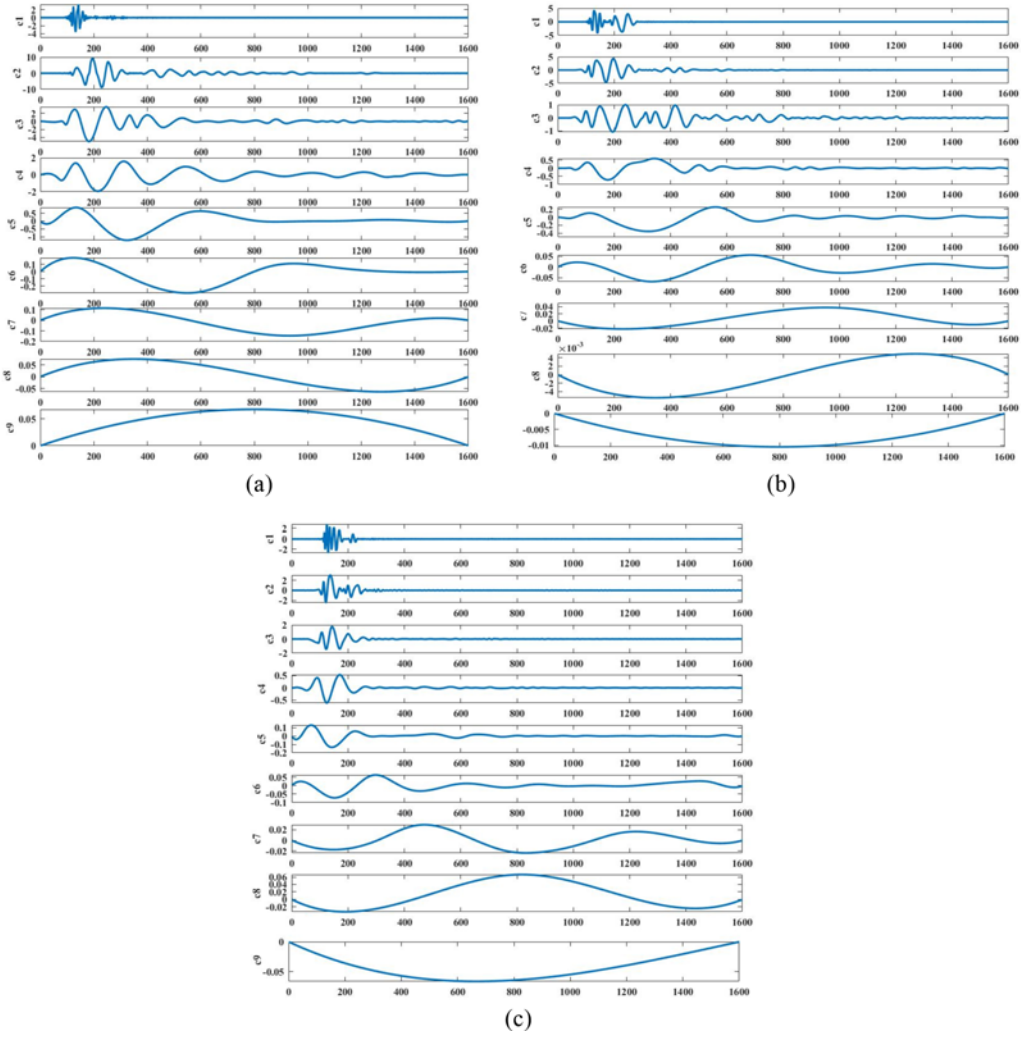

Fig. 8. Imf Components of the Vibration Waveforms: (a) EMD of V4, (b) EMD of V3, (c) EME of V2

from a high to a low frequency. The decomposition stopped when it became impossible to continue at very low frequencies, and all EMD waveforms were obtained. It was seen in Fig. 8 that all sensor vibration signals are decomposed into 9 IMF components. A major part as a percentage for the first three components of the energy of the vibration was distributed above 90%. But as the distance to the point where the vibration occurs grows, the total amount of energy becomes smaller, and the number of components obtained generally decreases. Furthermore, the first three components can be seen to be higher in frequency than the later ones, and the reduction of energy at different frequency bands was known from the percentage of all components.

3.3.2 Signature Mass Spectrometry Waveforms

Figure 9 illustrates the distribution in frequency of the vibration signal obtained when transforming the components. The vibration energy is mainly distributed at 0 – 100 Hz and concentrated at 0 – 30 Hz. With the increase of focal distance, the amplitude shows a downward trend as a whole, from 2.50 m to 11.28 m, and the peak value of amplitude decreases to 53%. The overall signal attenuation was very high at 95% close to the point of vibration, suggesting that structural safety should be more concerned in the area within 5 m of the point of vibration. As the focal length increases, high frequency energy gradually dominates. The characteristics of HHT analysis are more obvious than fast Fourier transform.

3.3.3 Instantaneous Energy Spectrum

As shown in Fig. 10, the x-axis of the instantaneous energy spectrum represents the sampling points and the y-axis represents the energy. The sampling frequency of this time is 100 Hz, there are 1000 sampling points within 1 s. From the figure, the distribution of energy in time can be observed. At closer distances, the peak energy decreases rapidly with increasing focal length. From 2.5 m to 11.28 m, the peak energy decreases by 63%. On V4 with the smallest focal distance, the energy is distributed at the sampling point of 0 – 1,600 and distributed in 1.6 s, mainly in 0 – 0.2 s.

3.3.4 Three Dimensional Hilbert Spectrum

Figure 11 is a three-dimensional Hilbert spectrogram, where the X, Y, and Z axes represent the sampling point, frequency, and energy, respectively. The abrupt change in energy represented a vibration event, with the peak value corresponding to the speed of vibration and the energy duration to the duration of the blast vibration. Compared with the Fourier spectrum, the discretization of HHT reflects that due to the existence of a priori function, there will be no continuous distribution of spatial spectral values caused by the increase of window such as Fourier transform.The

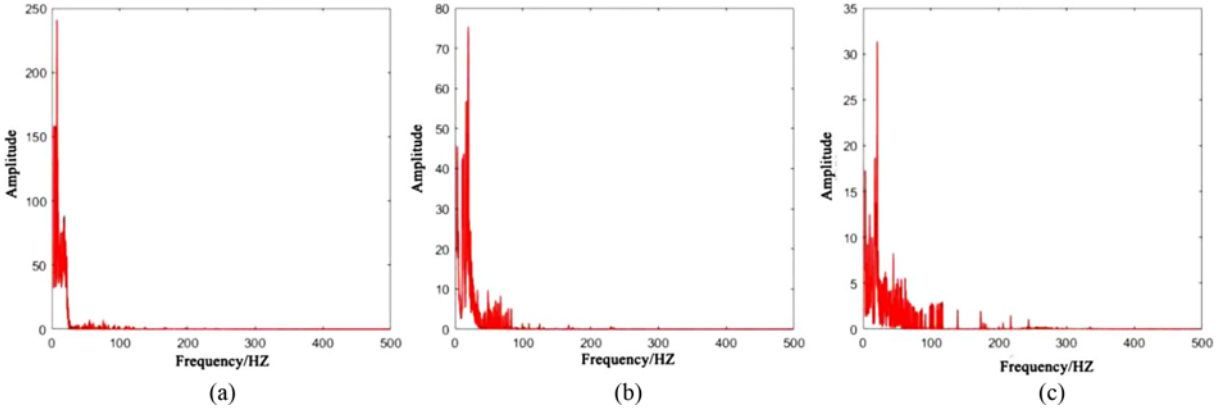

Fig. 9. Hilbert Marginal Amplitude Spectra: (a) Marginal Spectrum of V4, (b) Marginal Spectrum of V3, (c) Marginal Spectrum of V2

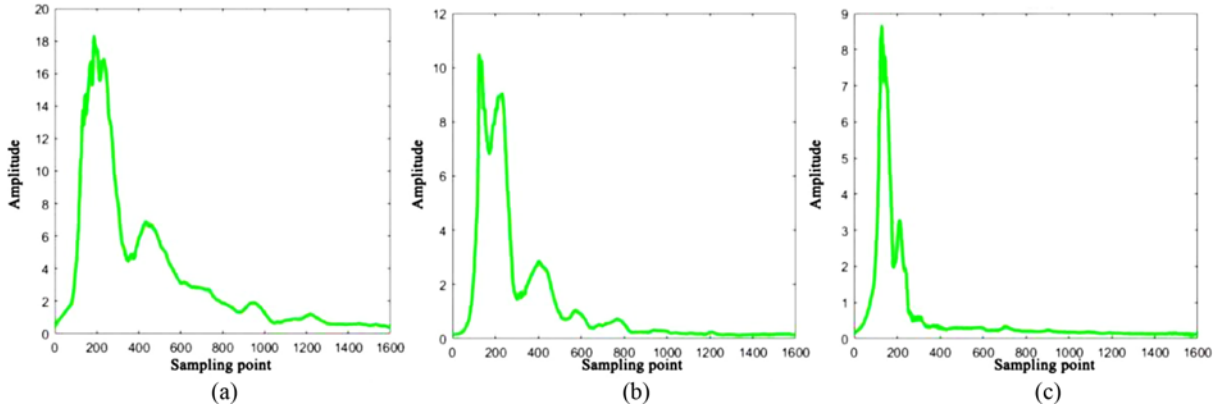

Fig. 10. Hilbert Instantaneous Energy: (a) Instantaneous Eenergy Spectrum of V4, (b) Instantaneous Energy Spectrum of V3, (c) Instantaneous Energy Spectrum of V2

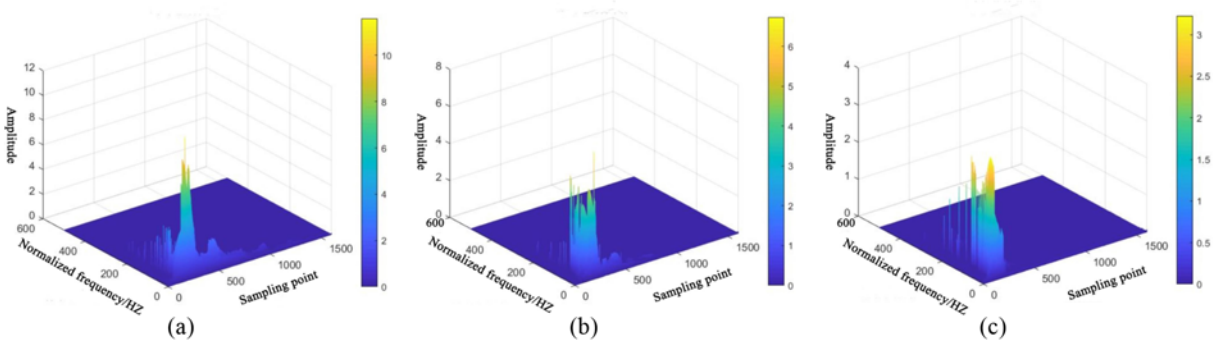

Fig. 11. Three-Dimensional Hilbert Spectra: (a) 3D Hibert Spectrogram of V4, (b) 3D Hilbert Spectrogram of V3, (c) 3D Hilbert Spectrogram of V2

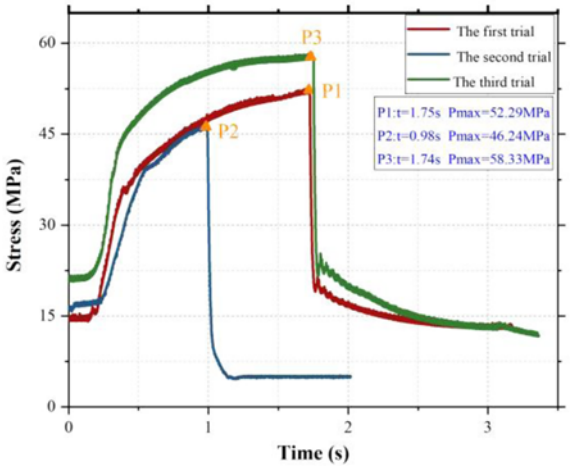

Fig. 12. Pressure Curve Diagram

peak energy corresponds to the amplitude of the vibration signal, that is, the peak vibration velocity, and the trend of the decay of the vibration velocity showed that the energy decays rapidly with increasing distance from the source. The energy is mainly distributed at 0 – 200 Hz and 0 – 1 s at the time point. With the increase of focal distance, the energy is dispersed in frequency and concentrated in time, which is consistent with the results of instantaneous energy spectrum and marginal spectrum.

3.4 Experimental Pressure Curves

The pressure curves for the three sets of experiments are shown in Fig. 12. Relief pressure was dependent on the thickness of the fracture tube weakness, the greater the thickness the higher the pressure. Observing the curves for the initial pressures of 15 – 22.5 MPa, each curve underwent a slow linear rise, reaching 30 – 45 MPa when the pressure rises gradually became slower, reaching a peak pressure after there was a slow fluctuating phase after the instantaneous pressure release. These curves were helpful in understanding the pressure rise process and the fracturing mechanism.

3.5 Calculation of TNT Equivalent

The type of fracturing tube used this time is the same, and the fracturing pressure measured by connecting the pressure sensor to the safety gas pipe was 60 MPa. In previous related studies (Hu et al., 2018; Yang et al., 2019b; Bai et al., 2020; Wang et al., 2020), the energy calculation formula is:

$$Eg=\frac{PV}{K-1}[1-(\frac{P_1^{\frac{K-1}{K}}}{P})], \tag{1}$$

where

Eg is the total energy of the explosion, kJ; P is the instantaneous fluid pressure released, MPa; V is the volume of the iron tube, m^3; K is the adiabatic index of the gas inside the tube, taking 1.295. Calculated result is 1272.313 KJ.

The approximate TNT equivalent W_{TNT} can be calculated using Eq. (2):

$$W_{TNT}=\frac{E_g}{Q_{TNT}} \tag{2}$$

Q_{TNT} is 1 kg TNT explosion energy, taking 4,250 kJ/kg. After calculation, the TNT equivalent of 1,000 mm cracking tube is 299.37 g.

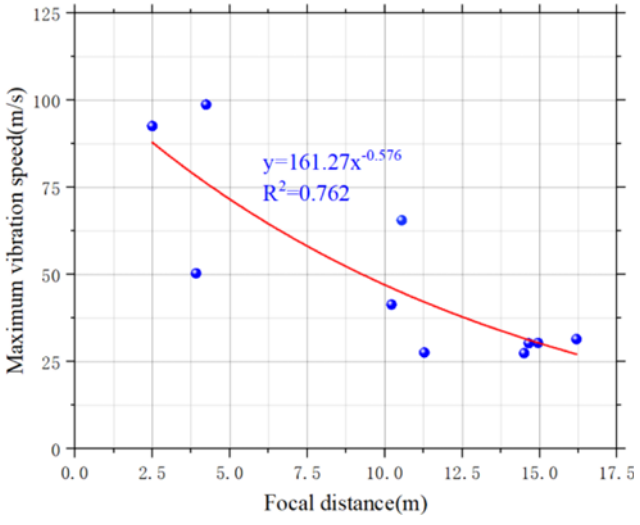

Fig. 13. Statistical Graph of Attenuation of Vibration Waveform Velocity with Source Distance

Table 3. Vibration Velocity of Safe Particle on Newly Poured Large-Volume Porch Foundation Surface

Age of cauldron(d)	0 – 3	3 – 7	7 – 28
Safe particle vibration velocity (mm/s)	15 – 20	20 – 50	50 – 70

4. Discussion

4.1 Analysis of Vibration Velocity Attenuation Law

Figure 13 illustrates the fitted curve of the peak decay of the vibration velocity resulting from the two vibration events. When the source distance reaches 3.91 m, the vibration velocity is 50.391 mm/s, which meets the vibration velocity requirements of safe particles in Table 3. Signal decay could be fitted to a multiplicative power function curve, the vibration decay rate decreases with increasing distance and the fitting accuracy is 0.82. Therefore, both can be used to predict the peak vibration velocity at different distances by the power function to determine whether it is dangerous or not. According to Fig. 13, damage can be divided into two areas based on fracture distribution characteristics, namely the zone of rapid reduction of vibration velocity (2.5 – 10 m) and the stable zone (>10 m). Vibrations increased the closer the distance, and the greater the rate of increase in vibration, making it more dangerous.

4.2 Comparison between Thermal Shock Rock Breaking with Dry Ice Powder and Drilling and Blasting Method

Figure 14 shows the typical vibration waveform and spectrum diagram of rock breaking by drilling and blasting method. The vibration attenuates to 0 in a short time, which represents the instantaneous release of energy by explosives (Xu et al., 2022). According to this rock-breaking mechanism, the blast-induced stress wave action acts first on the rock mass and the high strain rate compressional-tensile action is applied first. The action of blasting gas is considered to have a lower strain rate and it acts to extend the fracture along the initial fracture created by the stress wave. This extension includes fracture extension and an increase in fracture width (Jayasinghe et al., 2019). This blast mechanism is accepted by most researchers and the study of fracture mechanisms can be advanced by considering the important factors together and distinguishing the role of important factors and their contribution to rock damage (Wang et al., 2021). Thermal shock with dry ice powder was a physical change, with the blasting products containing only non-toxic carbon dioxide gas, while blasting with conventional rock emulsion explosives was a chemical change, generating large amounts of toxic and harmful gases such as CO, NO, NO_2, N_xO_y and Sulphur-oxygen compounds during the explosion. From the energy calculations and vibration measurements, the

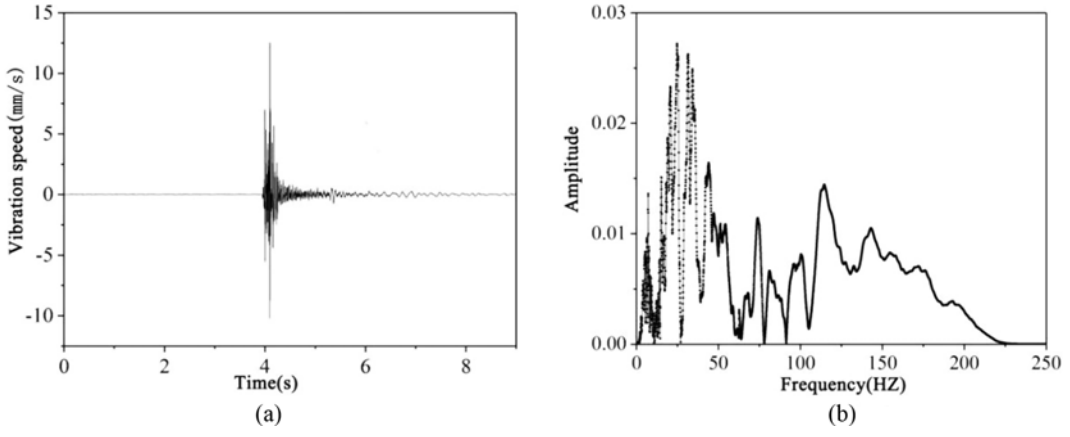

Fig. 14. Explosive Blasting Waveform and Spectrum: (a) Typical Vibration Waveforms of Explosive Blasting; (b) Frequency Distribution of Vibration Energy in Explosive Blasting

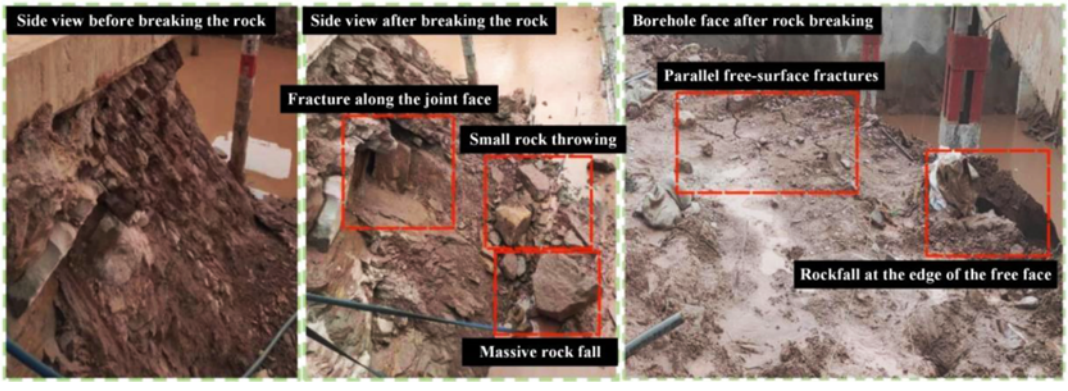

Fig. 15. On-Site Rock Breaking Pictures

low energy density and weak vibration of dry ice powder thermal shock rock breaking was suitable for use in construction in sensitive areas such as urban public works.

Therefore the process of rock destruction cannot be explained by the traditional theory of the combined action of blasting stress waves and blasting gas. As can be seen from Fig. 15, the damage at the orifice location of the rock-breaking hole was not obvious after the dry ice thermal shock broke the rock, with only a few small size fissures, but obvious macro cracks are formed around the borehole. Observation of the experimental specimen fracture pattern, as shown in Fig. 16, revealed that in addition to the high energy gas leakage producing a radial main fracture, fracture bifurcation, and surface detachment an annular fracture was also present on one face of the specimen. Fig. 17 demonstrated the fracturing principle and the fracturing effect of thermal shock breaking of the rock by dry ice powder. Three zones with different damage characteristics were identified, the fracture zone where the rock was broken and essentially separated, the fracture zone where radial fractures were evident, and the vibration-affected zone where no damage was evident, but vibration waves were distributed internally. Based on the pressure profile and fracture distribution combined with fracture mechanics, it was obtained that, unlike explosives, the new technique produces a small fracture zone, the extent of the fracture zone is related to the pressure and mass of the high-energy gas, and the vibration-affected zone is much smaller than that of explosive blasting (Yan et al., 2021). There is no obvious crushing area around the borehole, and the main failure form is the macro cracks around the borehole. Based on the form of rock damage in the field, a small amount of fractured free-surface rock throw at the orifice with gas venting, the dry ice powder thermal impact rock breaking is divided into three stages: the first stage corresponds to a high strain rate stress wave acting on the center of the blast, the reflection of the stress wave on the free-surface, is also a dynamic rock breaking process. The third stage corresponds to the expansion of the radial cracking process caused by the high-energy CO_2 fluid, i.e. the air wedge effect. In this stage, the rock is thrown after the initial fracture extension of the rock mass is complete, while the gas is released.

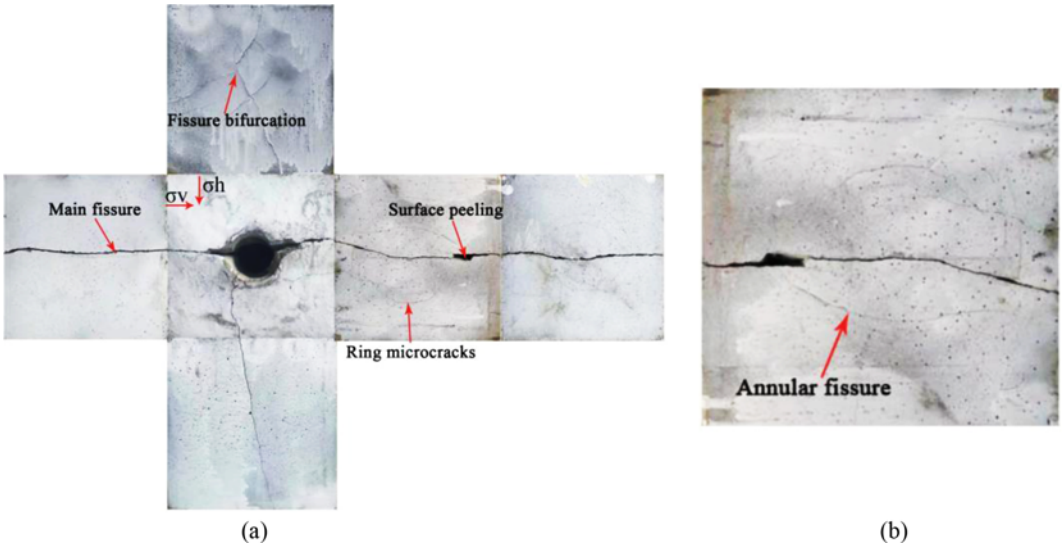

Fig. 16. Specimen Fracture Distribution Diagram: (a) Expanded View of Damaged Specimen, (b) Circumferential Fracture Diagram

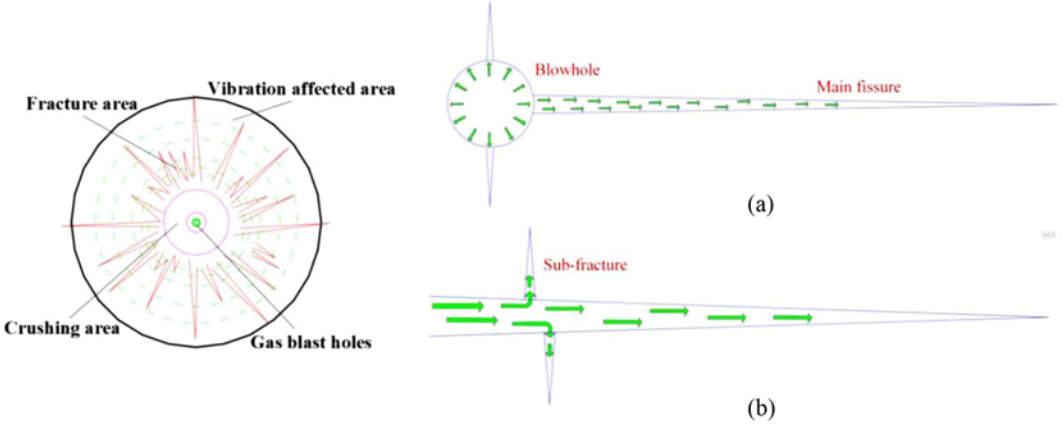

Fig. 17. Schematic Diagram of the Principle of CO_2 Phase Change Fracturing Technology: (a) High-Energy Fluids Extend Initial Fissure, (b) High-Energy Fluids Create Sub-fissures

Compared with mechanical rock breaking, it can improve the rock breaking efficiency of tunnel construction; Compared with rock breaking by drilling and blasting, the vibration has less influence on the tunnel structure and is safer.

4.3 Dynamic Parameters and Safety Assessment

The characteristics of the vibration signals obtained from the HHT analysis were evident, with the degree of three-dimensional concentration of energy observed in Fig. 11. The densely distributed volume of energy was the main source of vibration damage, and it is of great interest how to eliminate this energy and assess the damage caused by this energy.The EMD decomposition was very objective, and the results were more credible, which was very significant for the safety evaluation.

The observation of energy density searched for the most energy dense areas, mainly in the first 100 sampling points, with dominant frequencies in the low frequency range not exceeding 200 Hz. As the distance from the source increases, the energy becomes more dispersed in frequency and more concentrated in time. The lower the frequency of vibration (5 − 10 Hz) the better the breaking effect can be for rock breaking, as the resonance effect is more likely to produce internal damage. For structural safety low frequency signals would be very dangerous, but low frequency signals decay quickly which is beneficial for structural protection (Li et al., 2020c). Low frequency energy can cause more serious damage to buildings due to resonance effects. It would be insufficient to use only the peak vibration velocity as the evaluation indicator for the protection of a structure, the influence of the main frequency and duration of vibration cannot be ignored. Frequency of vibration also provides an important factor in the assessment of damage. Since fatigue damage reduces the strength of a structure, a higher breaking efficiency means a lower number of vibrations.When the focal distance is small, the vibration energy is more dispersed in time, because the action time of air wedge is longer than that of traditional drilling and blasting method, the energy release time is long and the peak value is low, which is safer than drilling and blasting method. The maximum vibration tested on the support concrete was 101.395 mm/s, which is sufficient to meet the protection requirements, but the frequency distribution also needs attention. On the support ridge, the safety distance of dry ice powder thermal shock rock breaking technology is less than 11 m.

5. Conclusions

1. The peak vibration speed was below 50 mm/s for concrete structures safe as long as it was farther than 10 m from the burst hole in the support concrete. The noise was only 83 dB at 4 m, which had little impact on the life of the surrounding residents;
2. The thermal shock breaking with dry ice powder increased the efficiency of rock breaking in tunnel construction compared to mechanical rock breaking. The vibrations had a smaller impact range and have a smaller and safer impact on the tunnel construction structure than drilling and blasting methods;
3. The new rock-breaking technology induced damage can be divided into three regions, with radial fractures generated by high-energy fluids dominating.Compared with rock breaking by drilling and blasting, the vibration has less influence on the tunnel structure and is safer;
4. In contrast to Fourier transform analysis, HHT was more suitable for processing vibration signals and its energy distribution in time and frequency was a promising reference for safety evaluation

Acknowledgements

This work is supported by the Key Program of National Natural Science Foundation of China (51934007), the Major Scientific and Technological Innovation Program in Shandong Province (2019JZZY020505) and a Project Funded by the Priority Academic Program Development of Jiangsu Higher Education Institutions (PAPD).

ORCID

Shaobin Hu https://orcid.org/0000-0001 -5313-2646

References

Babu TR, Srikanth S, Sekhar AS (2008) Hilbert-Huang transform for detection and monitoring of crack in a transient rotor. *Mechanical Systems and Signal Processing* 22(4):905-914, DOI: 10.1016/j.ymssp.2007.10.010

Bai X, Zhang DM, Zeng S, Zhang SW, Wang DK, Wang FL (2020) An enhanced coalbed methane recovery technique based on CO_2 phase transition jet coal-breaking behavior. *Fuel* 265:116912, DOI: 10.1016 / j.fuel.2019.116912

Chang J, Sun L, Dai B, Li H, Liu Z, Zhao X, Ke B (2023) Research on the fracture properties and mechanism of carbon dioxide blasting based on rock-like materials. *Minerals* 13(1):3, DOI: 10.3390/min13010003

Chen SL, Huang BX, Zhao XL, Lu WY, Tian ZC (2020) Directional fracturing excavation technology based on liquid CO_2 phase transition infreezing shaft sinking. Energy Sources, Part A: Recovery, Utilization, and Environmental Effects, DOI: 10.1080/15567036.2020.1862366

Chen HD, Wang ZF, Qi LL, An FH (2017) Effect of liquid carbon dioxide phase change fracturing technology on gas drainage. *Arabian Journal of Geosciences* 10:314, DOI: 10.1007/s12517-017-3103-0

Goodarzi M, Mohammadi S, Jafari A (2015) Numerical analysis of rock fracturing by gas pressure using the extended finite element method. *Petroleum Science* 12:304-315, DOI: 10.1007/s12182-015-0017-x

Hu GZ, He WR, Sun M (2018) Enhancing coal seam gas using liquid CO_2 phase-transition blasting with cross-measure borehole. *Journal of Natural Gas Science and Engineering* 60:164-173, DOI: 10.1016/j.jngse.2018.10.013

Hu S, Pang S, Yan Z (2019) A new dynamic fracturing method: Deflagration fracturing technology with carbon dioxide. *International Journal of Fracture* 220:99-111, DOI: 10.1007/s10704-019-00403-8

Huang D, Cui S, Li XQ (2019) Wavelet packet analysis of blasting vibration signal of mountain tunnel. *Soil Dynamics and Earthquake Engineering* 117:72-80, DOI: 10.1016/j.soildyn.2018.11.025

Jayasinghe LB, Shang JL, Zhao ZY, Goh ATC (2019) Numerical investigation into the blasting-induced damage characteristics of

rocks considering the role of in-situ stresses and discontinuity persistence. *Computers and Geotechnics* 116:103207, ISSN 0266-352X, DOI: 10.1016/j.compgeo. 2019.103207

Kumar S, Mishra AK (2020) Reduction of blast-induced ground vibration and utilization of explosive energy using low-density explosives for environmentally sensitive areas. *Arabian Journal of Geosciences* 13(14), DOI: 10.1007/s12517-020-05645-8

Lee JS, Sung KA, Myung SG (2016) Attenuation of blast vibration in tunneling using a pre-cut discontinuity. *Tunnelling and Underground Space Technology* 52:30-37, DOI: 10.1016/j.tust.2015.11.010

Li ZY (2021) Study on vibration effect of pre-splitting crack in tunnel excavation under thermal explosion loading. *Case Studies in Thermal Engineering* 28:101401, DOI: 10.1016/j.csite. 2021.101401

Li QY, Chen G, Luo DY, Ma HP, Liu Y (2020a) An experimental study of a novel liquid carbon dioxide rock-breaking technology. *International Journal of Rock Mechanics and Mining Sciences* 128:104244, DOI: 10.1016/j.ijrmms.2020.104244

Li Q, Gao ZH, Xu WL, Wang K, Liu S, Ran GF, Hu Y (2020b) Experimental research on the dynamic propagation process of mode I cracks in the rock under directional fracture blasting using the strain gauge method. *Engineering Fracture Mechanics* 35:107113, DOI: 10.1016/j.engfracmech.2020.107113

Li SS, Xiang P, Wei B, Yan L, Xia Y (2020c) A nonlinear static procedure for the seismic design of symmetrical irregular bridges. *Shock and Vibration* 8899705, DOI: 10.1155/2020/8899705

Nguyen H, Bui XN, Tran QH, Moayedi H (2019) Predicting blast-induced peak particle velocity using BGAMs, ANN and SVM: A case study at the Nui Beo open-pit coal mine in Vietnam. *Environmental Earth Sciences* 78:479, DOI: 10.1007/s12665-019-8491-x

Skeberis C, Zaharis ZD, Xenos TD, Spatalas S, Arabelos DN, Contadakis ME (2015) Time-frequency analysis of VLF for seismic-ionospheric precursor detection: Evaluation of Zhao-Atlas-Marks and Hilbert-Huang Transforms. *Physics and Chemistry of the Earth, Parts A/B/C* 85:174-184, DOI: 10.1016/j.pce.2015.02.006

Song SG, Li SC, Li LP, Shi SS, Zhou ZQ, Liu ZH, Shang CS, Sun HZ (2019) Model test study on vibration blasting of large cross-section tunnel with small clearance in horizontal stratified surrounding rock. *Tunnelling and Underground Space Technology* 92:103013, DOI: 10.1016/j.tust.2019.103013

Tao R, Zhang F, Wang Y (2008) Research progress on discretization of fractional fourier transform. *Science in China, Series F: Information Sciences* 51:859-880, DOI: 10.1007/s11432-008-0069-2

Umit O (2008) Environmental impacts of ground vibration induced by blasting at different rock units on the Kadikoy–Kartal metro tunnel. *Engineering Geology* 100:82-90, DOI: 10.1016/j.enggeo.2008.03.006

Wang XF, Hu SB, Wang EY, Zhang Q, Liu B (2022a) Extraction of vibration waveform characteristics of dry ice powder pneumatic rock breaking using Hilbert-Huang transform. *Arabian Journal of Geosciences* 15:71, DOI: 10.1007/s12517-021-09236-z

Wang ZL, Konietzky H (2009) Modelling of blast-induced fractures in jointed rock masses. *Engineering Fracture Mechanics* 76(12):1945-1955, DOI: 10.1016/j.engfracmech.2009.05.004

Wang X, Li JC, Zhao XB, Liang Y (2022b) Propagation characteristics and prediction of blast-induced vibration on closely spaced rock tunnels. *Tunnelling and Underground Space Technology* 123:104416, DOI: 10.1016/j.tust.2022.104416

Wang XF, Hu SB, Wang EY, Zhang Q, Liu B (2023) Experimental research and energy analysis of a new type of dry ice powder pneumatic rock breaking technology. *International Journal of Mining Science and Technology*, DOI: 10.1016/j.ijmst.2022.12.010

Wang S, Tan X, Xia Y, Tian B, Liang B (2021) Progress on modeling of dynamic productivity of fractured gas condensate reservoir based on a fluid-solid coupling method. *Frontiers of Earth Science* 9:722787, DOI: 10.3389/feart.2021.722787

Wang B, Liu SD, Sun HC, Ding X, Jin B, Zhang ZD (2020) Supercritical CO_2 source for underground seismic exploration. *Journal of King Saud University - Science* 32:1731-1737, DOI: 10.1016/j.jksus.2020.01.010

Wen YC, Ming Q, Hou JR, Liang T, Raj I, Ma SX, Yuan N (2019) Experimental study on nitrogen drive and foam assisted nitrogen drive in varying-aperture fractures of carbonate reservoir. *Journal of Petroleum Science and Engineering* 180:994-1005, DOI: 10.1016/j.petrol.2019.06.028

Wu ZH, Huang NE (2004) A study of the characteristics of white noise using the empirical mode decomposition method. *Proceedings of the Royal Society A* 460:1597-1611, DOI: 10.1098/rspa.2003.1221

Wu XD, Min G, Wu HJ, Liu XY (2021) Parameter calculation of the initiating circuit with mixed use of nonel detonators and electronic detonators in tunnel controlled-blasting. *Tunnelling and Underground Space Technology* 113:103975, DOI: 10.1016/j.tust.2021.103975

Xia YQ, Jiang N (2019) Safety assessment of upper water pipeline under the blasting vibration induced by Subway tunnel excavation. *Engineering Failure Analysis* 104:626-642, DOI: 10.1016/ j.engfailanal.2019.06.047

Xia X, Li HB, Liu YQ, Yu C (2018) A case study on the cavity effect of a water tunnel on the ground vibrations induced by excavating blasts. *Tunnelling and Underground Space Technology* 71:292-297, DOI: 10.1016/j.tust.2017.08.026

Xu P, Yang R, Zuo J, Ding CX, Chen C, Guo Y, Fang SZ, Zhang YF (2022) Research progress of the fundamental theory and technology of rock blasting. *International Journal of Minerals Metallurgy and Materials* 29:705-716, DOI: 10.1007/s12613-022-2464-x

Yan H, Zhang J, Li B, Zhu C (2021) Crack propagation patterns and factors controlling complex crack network formation in coal bodies during tri-axial supercritical carbon dioxide fracturing. *Fuel* 286, DOI: 10.1016/j.fuel.2020.119381

Yang XF, Li YH, Nie AG, Zhi S, Liu LY (2020) Numerical study on rock breaking mechanism of supercritical CO_2 jet based on smoothed particle hydrodynamics. *Computer Modeling in Engineering & Sciences* 122(3):1141-1157, DOI: 10.32604/cmes.2020.08538

Yang GD, Wang GH, Lu WB, Yan P, Chen M (2019a) Damage assessment and mitigation measures of underwater tunnel subjected to blast loads. *Tunnelling and Underground Space Technology* 94:103131, DOI: 10.1016/j.tust.2019.103131

Yang XL,Wen GC, Sun HT, Li XL, Lu TK, Dai LC, Cao J, Li L (2019b) Environmentally friendly techniques for high gas content thick coal seam stimulation-multi-discharge CO_2 fracturing system. *Journal of Natural Gas Science and Engineering* 61:71-82, DOI: 10.1016/j.jngse.2018.11.006